Epitaxial growth and magnetic properties of Fe(111) films on Si(111) substrate using a GaSe(001) template

M. Eddrief, Y. Wang, and V. H. Etgens
Laboratoire de Minéralogie et de Cristallographie de Paris-CNRS-Universités Paris VI et VII, 4 Place Jussieu, F-75252 Paris Cédex 05, France

D. H. Mosca,* J.-L. Maurice, J. M. George, and A. Fert
Unité Mixte de Physique CNRS-Thomson, Domaine de Corbeville, 91404 Orsay, France

C. Bourgognon
Laboratoire de Spectrométrie Physique, Université Joseph Fourier Grenoble-CNRS, Boîte Postale 87, 38402 Saint Martin d'Hères Cédex, France

(Received 2 August 2000; published 13 February 2001)

We report the growth of Fe(111) overlayers on unstrained GaSe(001) epitaxied on a Si(111)-H terminated substrate. The GaSe prevents chemical reaction between Fe and Si and enables the achievement of fully relaxed Fe films above monolayer coverage, despite the 8% lattice mismatch between Fe and GaSe. The evolution of the magnetic properties and chemical reactivity of the iron layer has been studied as a function of thickness. The reduction of magnetization for very thin Fe films has been correlated with a self-limited solid-state reaction at the Fe/GaSe interface.

DOI: 10.1103/PhysRevB.63.094428 PACS number(s): 75.70.Cn, 79.60.Jv, 81.15.Hi

I. INTRODUCTION

The direct integration of ferromagnetic thin films on semiconductors is more than just a growth challenge, it is also a way to take advantage of the two spin states of the electrons leading to hybrid spin-injection devices for microelectronics.[1,2]

Currently, the majority of experiments with hybrid ferromagnetic/semiconductor heterostructures deals with the systems such as Fe/GaAs,[3] Fe/ZnSe,[4] and Mn-based compounds grown on GaAs and Si substrates.[5–8] Despite the majority of solid-state devices that are presently being made using Si as the semiconductor, only a few works have been devoted to the Fe/Si system,[9,10] which is inherently complex due to various problems.

It was shown that epitaxial growth of ferromagnetic metals is possible on H-terminated Si surfaces, although most ferromagnetic/silicon interfaces are reactive. In this case, stable and metastable silicides are formed after metal deposition by solid-state interdiffusion,[10] even at room temperature. In the Si-based technology, its native oxide could be used as an insulating and interdiffusion barrier, but the $Si\text{-}SiO_2$ interface is not atomically flat, thus destroying the epitaxial ordering of subsequent metal deposition. A high-quality CaF_2 epilayer grown on Si(111) substrates[11] has been considered as a suitable alternative for SiO_2 since it produces an atomically flat interface. Although Fe grows epitaxially on CaF_2, the Fe/CaF_2 growth proceeds by three-dimensional islanding rather than continuous film covering.[12] Besides, ferromagnetism is only observed when the Fe island radius is larger than 3 nm, a chemical reaction between Fe and CaF_2 being rejected from thermochemical considerations.[13]

In a previous work, the epitaxial growth of very thin GaSe films on various Si(111) surfaces has been reported using molecular-beam epitaxy (MBE).[14–17] GaSe is a lamellar semiconductor with a γ-rhombohedral structure consisting of a hexagonal Se-Ga-Ga-Se stacking sequence along the [001] direction[18] (hereafter, this latter sequence is called an elemental sheet of GaSe with a thickness of 7.95 Å). The atoms in a sheet are bound to each other through ionocovalent forces, whereas the sheets are held together via weak van der Waals-like forces. All bonds are confined within the sheet with its surface being terminated by Se atoms and arranged in a sixfold triangular lattice with a Se-Se distance of 3.755 Å.[18] From the van der Waals character of the intersheet interactions, one could expect that the strain lattice mismatch (-2.6%) between GaSe and Si is accommodated through the first van der Waals gap [by half of a GaSe sheet strained to an Si(111) surface followed by upper relaxed sheets].[14–17] In such a way, the lamellar GaSe films on Si(111) are expected as helpful in growing materials that are hardly compatible with Si and could even be used to avoid the reactivity between Fe and Si that conspicuously form stable and metastable compounds with Si.[10]

In this study, we report on the epitaxial growth, strain relaxation, and magnetic properties of body-centered-cubic Fe (α-Fe) films on a 20-Å-thick GaSe(001) grown on a H-terminated Si(111) substrate. 100-Å-thick ZnSe overlayers were used to prevent Fe oxydation. Fe(111)/GaSe(001) epilayers on an Si(111) substrate have been prepared using standard MBE conditions.

II. EXPERIMENT

Nominal Si(111) ($\rho \sim 10\,\Omega$ cm) wafers have been used as substrates for these experiments. In order to promote γ-type GaSe films[14–17] the growth has been performed on an ordered hydrogenated Si(111) surface[19] following a procedure described elsewhere.[14,16] The GaSe has been deposited by coevaporating Ga and Se from solid source Knudsen cells in

 ©2001 The American Physical Society

a Riber 32 MBE system, with a base pressure below 10^{-10} T. The Se/Ga flux ratio was selected around ~8, which provides a growth rate of about 11 Å/s, while the substrate temperature was kept at 450 °C. The GaSe(001) film thickness was fixed at 20 and 12 Å for x-ray photoelectron spectroscopy (XPS) and transmission electron microscopy (TEM), respectively, corresponding to a fully relaxed GaSe epilayer,[14–17] and exhibiting van der Waals gaps (two or one, respectively) through which the strain of the Fe overlayer could be relaxed in respect to the Si substrate.

The Fe deposition has been performed as follows. First, the substrate temperature was raised to 120 °C, which is the lowest temperature for obtaining good epitaxial Fe films. The iron was deposited with a growth rate close to 1.3 Å/min [i.e. ~0.8 ML/min since 1 ML = 1.65 Å of α-Fe(111)] and thicknesses ranging from 0.65 to 1000 Å. The growth rate was evaluated (within an uncertainty of about 10%) by cross-sectional TEM images. After the deposition, each sample was cooled down to room temperature, and a 100 Å ZnSe cap layer was deposited on each sample. This procedure has been tested as very efficient to protect samples from oxidization under ambient atmosphere for a few months.

In-situ reflection high-energy electron diffraction (RHEED) measurements were performed using a variable incidence Staib RHEED system operating at 12 keV under a grazing angle (below 1°). For quantitative analysis, the diffraction pattern was recorded on a fluorescent screen using a high-sensitivity charge-coupled-device (CCD) camera linked to a computer image-processing system. Streak positions and distances were measured as a function of time by making an intensity profile along a predefined region. The peaks were numerically analyzed thus enabling an accuracy of a few tenths of a percent in the lattice parameter determination.

In-situ x-ray photoelectron spectroscopy (XPS) has been used to probe the core level of the chemical species. At several stages of deposition, the samples were cooled down to room temperature and transferred to an XPS chamber under UHV. The XPS spectra were taken with a Mac II spectrometer using a Mg anode (1253.6 eV). The photoelectrons were collected at an average exit angle of 43° from the sample normal. The overall energy resolution was about 1.27 eV [as measured by the full width at half maximum (FWHM) of an Ag-$3d_{5/2}$ photoelectron line]. Ga-$2p_{3/2}$, Se-$3p$, Se-$3d$, and Ga-$3d$ (for the GaSe epilayer); Si-$2p$ (for the Si substrate); and Fe-$2p_{3/2}$, Fe-$3s$, and Fe-$3p$ (for the Fe overlayer) core levels were collected and analyzed as a function of iron thickness [over the 20-Å-thick GaSe(001)/Si(111)]. Since the effective photoelectron escape depths of Ga-$2p_{3/2}$ and Ga-$3d$ are estimated at ~5.2 and ~17.6 Å, respectively,[20] one can assume that Ga-$3d$ photoelectrons probe all Ga atomic planes of the 20-Å-thick GaSe film (five atomic planes of Ga and five atomic planes of Se). In contrast, the Ga-$2p_{3/2}$ photoelectrons probe only subatomic planes near the surface of the film. We report only Ga-$3d$ spectra results in order to follow the evolution of all Ga atomic planes during the Fe/GaSe interface formation. Also, by assuming that the escape depth of Si-$2p$ and Ga-$3d$ photoelectrons are quite close due to their close kinetic energies, the 20 Å GaSe does not completely screen the Si-$2p$ photoelectrons [30% emission for bare H-terminated Si(111) substrate[17]]. Thus, the Si-$2p$ core level has been used to probe the Si surface stability below the GaSe epilayer in respect to the silicide formation during the Fe deposition.

The crystalline structure of the Fe films has been investigated by x-ray diffraction (XRD) with θ-2θ scans using CuK_α radiation.

The magnetic properties of the iron films were probed by using an alternating-gradient force magnetometer (Princeton Measurements Corporation Micromag) and a superconducting quantum interference device (SQUID) magnetometer (Quantum Design MPMS) with magnetic fields applied along the $[1\bar{1}0]$, $[11\bar{2}]$, and [111] axes of Si. All magnetic measurements were performed on samples prepared with the same above-mentioned conditions with the only varying parameter being the iron thickness. The magnetic response of the Fe films has been studied by measuring the magnetic saturation moment per area of the Fe layer versus its thickness using the SQUID magnetometer operating at 30 K in magnetic fields up to 40 kOe. No significant change is observed on the saturation magnetic moment of the Fe films grown onto ZnSe and covered with a ZnSe capping layer deposited at room temperature.[21] Thus, we will focalize on the magnetic properties of the Fe/GaSe interface.

The sample diamagnetic signal was removed by a numerical fit from the ferromagnetic response of the Fe films. However, the magnetic response of the Fe films thinner than 78 Å showed a low remanence and its magnitude became similar to the diamagnetic signal. A reacted interfacial layer and ultimately the characteristic two-dimensional (2D) island growth of the Fe dominated the magnetic response at low Fe coverage.

III. RESULTS AND DISCUSSION

A. Epitaxy and structure

The RHEED diffraction has been monitored during the growth of Fe thin films on a GaSe epilayer. Figures 1(a) and (b) show the RHEED diagram taken along $[1\bar{1}0]$ and $[11\bar{2}]$ azimuths, respectively [direction labeled with respect to the (111) surface of silicon] after growth of 20-Å fully relaxed GaSe epitaxied on H-terminated Si(111) substrate.[14,17] These two main directions differ from each other by 30° and the $[21\bar{3}0]_{GaSe}$ streak spacing (which is parallel to $[11\bar{2}]_{Si}$ is larger by a $\sqrt{3}$ factor when compared to the $[10\bar{1}0]_{GaSe}$ one (parallel with $[1\bar{1}0]_{Si}$). The beginning of the Fe deposition at 120 °C is characterized by the GaSe 2D diffraction (streak patterns) that fades into an increasing background without, however, complete disappearance. In this diagram, the Bragg diffraction spots of Fe appear superimposed above 1 Å thickness. This spotlike feature (i.e., 3D diffraction) indicates that Fe islands dominate the early stages of growth. Once the Fe coverage increases, the Fe spots are considerably elongated but still superimposed with a spotty diagram. At around 7-Å Fe coverage (~4 ML), one observes that the streak pattern becomes sharper in spite of the persistence of the Bragg spots. No other RHEED pattern changes are observed with subsequent growth as illustrated in Figs. 1(c) and (d), taken

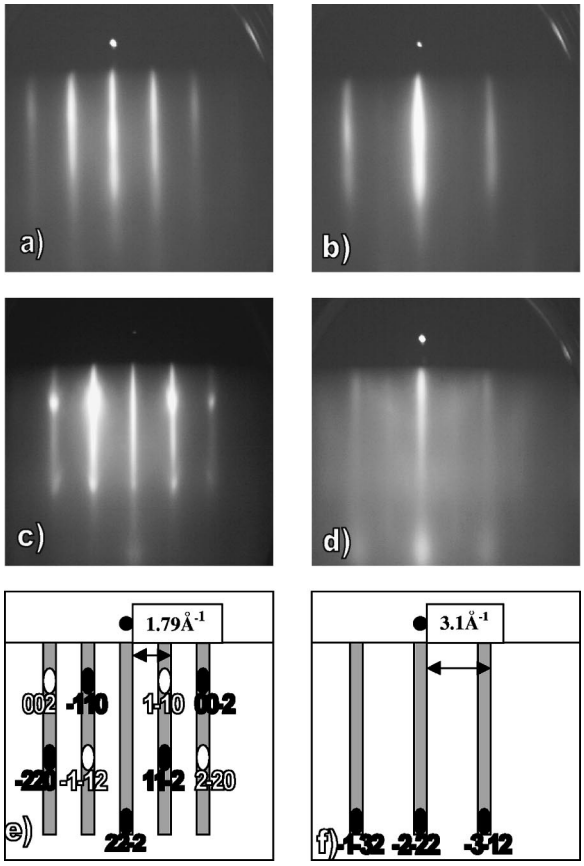

FIG. 1. (a) RHEED patterns of the 20-Å-thick GaSe surface taken along $[1\bar{1}0]_{Si}$ and (b) $[11\bar{2}]_{Si}$ azimuths, respectively. (c) and (d) RHEED patterns of a 91-Å-thick Fe film taken at the same azimuths shown in (a) and (b), respectively. (e) and (f) RHEED diagram schemes identifying Bragg diffraction spots of the Fe film from the reciprocal lattice of α-Fe(111) along $[1\bar{1}0]_{Fe}$ and $[11\bar{2}]_{Fe}$ (30° apart) azimuths, respectively, for *A* type ''oriented'' (open ellipses) and *B* type ''twinned'' (full ellipses) obtained by 180° rotation of *A* type around its [111] axis.

from a 91-Å-thick Fe film. Similar to a GaSe(001) surface, the Fe diagram shows two main in-plane azimuths that differ from each other by 30°; the streak spacing along $[11\bar{2}]_{Fe}$ being larger by a $\sqrt{3}$ factor than that of the pattern along $[1\bar{1}0]_{Fe}$. The Fe thin film shows a surface sixfold symmetry axis. It is important to emphasize that the appearance of the three-dimensional diffraction spots for thick Fe films reflects a roughening of the Fe film surface. This behavior is similar to the surface morphology observed by scanning tunneling microscopy for Fe/Fe(100) homoepitaxy[22] in which the surface is formed by mosaic mounds. Such mounds are developed in the earliest stages of the growth and continue through thicker films.[22,23]

Figures 1(e) and (f) display the RHEED diagram schemes that help to identify the Bragg diffraction spots associated with the reciprocal lattice of a α-Fe(111) film as taken along $[1\bar{1}0]_{Fe}$ and $[11\bar{2}]_{Fe}$ (30° apart) azimuths, respectively. As usual in the Fe(111) growth, the iron can adopt two different stacking sequences along the (111) direction during growth, which is the case when Fe is epitaxied on the Si(111) substrate, one aligned and the other one rotated by 180° in respect to the Si substrate.[24,25] If the film is perfectly 2D, the RHEED diagram is composed of streaks and, in this case, one cannot make a difference between the two twinned orientations. However, if one has a 3D pattern due to some surface roughness, as is the case of Fe here, one can distinguish two stacking sequences that will produce two different epitaxies. By considering Fig. 1(e), the aligned epitaxy (open ellipses) provides the reciprocal lattice point $1\bar{1}0$ on the right side of the Fe[111] axis [the Fe[111] axis is aligned in the (0,0) streak direction]. Conversely, the twinned epitaxy (filled ellipses) provides the reciprocal lattice point $\bar{1}10$ on the left side of the [111] axis. These two α-Fe orientations have a twinning relationship. Namely, the latter is the *B*-type structure that has a 180° rotation around its [111] axis relative of the *A*-type structure. According to the RHEED pattern shown in Fig. 1(c), these two orientations clearly exist but the twinned orientation seems to be predominant because the intensity of the $(\bar{1}10)$Fe spot is stronger than that of the $(1\bar{1}0)$Fe spot. In a 150-Å-thick Fe film, *B*-type orientation has been essentially evidenced by cross-sectional TEM analysis. Below, we summarize our results on the epitaxial Fe films grown on GaSe epilayer: matching plane relationship: (111)α-Fe//(001)GaSe//(111)Si; azimuthal orientation relationship: **A* type (aligned epitaxy): $[1\bar{1}0]\alpha$-Fe//$[10\bar{1}0]$GaSe//$[\bar{1}10]$Si; **B* type (twinned epitaxy): $[\bar{1}10]\alpha$-Fe//$[10\bar{1}0]$GaSe//$[\bar{1}10]$Si.

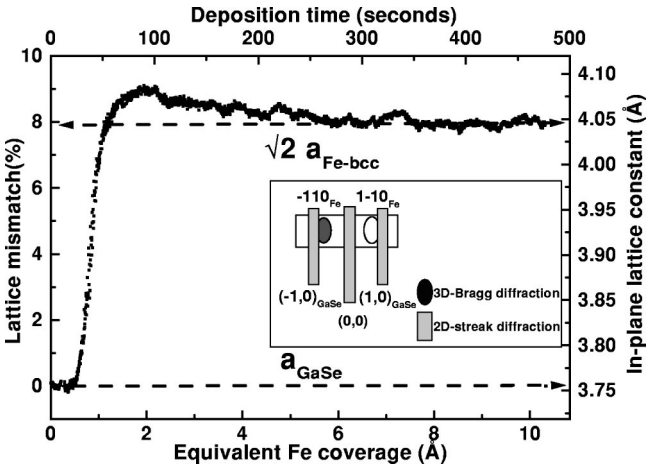

FIG. 2. In-plane lattice mismatch (left scale) as a function of the Fe equivalent coverage (deposition time is given in top axis), obtained from the profile analysis of the RHEED pattern. Sketch of the measured window profile of the RHEED pattern is shown in the inset. The spacing between the $(\bar{1},0)$ and (1,0) streaks of 20-Å-GaSe epilayer were used to normalize the results.

We have also followed the in-plane lattice parameter of the growing Fe film through the RHEED profiles using a high-sensitivity charge-coupled-device camera. The resulting in-plane lattice mismatch as a function of the equivalent Fe coverage (deposition time is given in the top axis) is presented in Fig. 2 with a thickness sampling of 0.005 Å taken along the $[1\bar{1}0]_{Si}$ azimuth ($[10\bar{1}0]_{GaSe}$ axis). The reference lattice parameter used for normalization was measured from GaSe $(\bar{1},0)$ and (1,0) streak spacing, which corresponds to

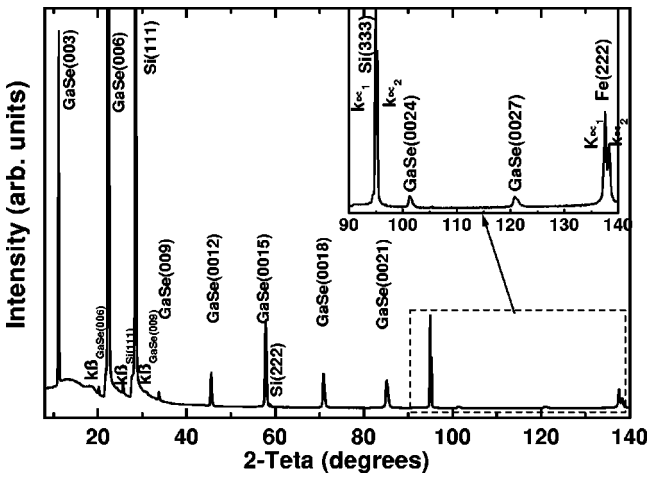

FIG. 3. X-ray diffraction pattern showing θ-2θ scan of a 1000-Å-thick Fe film grown on a 150-Å-thick GaSe epilayer previously grown on a Si(111) substrate. Bragg reflection peaks corresponding to the Fe film, GaSe epilayer, and Si substrate are identified.

$a^*_{\mathrm{GaSe}}=1.93\,\text{Å}^{-1}=2\pi/(a_{\mathrm{GaSe}}\cos 30°)$, where $\cos 30°$ takes into account the angular twisting between real and reciprocal lattices of a hexagonal surface. The in-plane lattice constant (right scale) is given in terms of the in-plane lattice constant of the bulk Fe, which is $\sqrt{2}$ times the (111) surface lattice constant (dashed line with double arrows on the plot). From the beginning of the growth, a quite-quick evolution is observed from $a_{\mathrm{GaSe}}=3.755$ Å to $a_{\mathrm{film}}=4.05$ Å. The measured a_{film} value [corresponding to $a^*_{\mathrm{film}}=2\pi/(\sqrt{2}a_{\alpha\text{-Fe}}\cos 30°)=1.79\,\text{Å}^{-1}$] is in very good agreement with the Fe bulk value, i.e., $a_{\alpha\text{-Fe}}=2.867$ Å, indicating that the Fe grew with its own lattice constant even on the monolayer regime, rather than straining to match the GaSe epilayer as it would be expected to in a usual heteroepitaxy. However, we note a small deviation of the in-plane lattice of the film between a thickness of 1 and 5 Å. This suggests the existence of an in-plane expansive strain ($\approx+0.6\%$) of the Fe overlayer directly in contact with GaSe epilayer. Photoemission studies presented in the next section reveal a chemical reactivity between the iron and GaSe at around 1.65 Å of coverage (corresponding to 1 ML) that corresponds to the maximum deviation observed in the in-plane lattice parameter. Apparently, a full-monolayer nucleation is needed to induce the chemical reaction between Fe and the topmost sheet of the GaSe epilayer. The formation of some compound can be responsible for the observed strain in the Fe islands. This lateral strain is probably accommodated at the interface in the first atomic planes of Fe(111).

The good crystal quality of the GaSe and Fe epilayers has been confirmed by XRD in θ-2θ scans. The XRD pattern of a 1000-Å-thick Fe film grown on GaSe(150 Å)/Si(111) is shown in Fig. 3. Only one Fe diffraction peak is observed, corresponding to the interplanar spacing of 0.827 Å, identified as the (222) reflection of α-Fe.[26] The rocking curve reveals a FWHM for this reflection of $\sim 0.3°$, which is comparable to the Si(333) peak. This small FWHM value of the α-Fe(222) Bragg reflection combined with the absence of any other Fe peaks confirms the good quality of iron thin films that have their (111) plane of α-Fe parallel to the (001) plane of the GaSe epilayer and to the (111) plane of the Si substrate. The (00l) peaks of the γ-rhombohedral structured GaSe epilayer were also observed underlying the Fe film, indicating the integrity of the GaSe epilayer after the Fe deposition.

B. X-ray photoelectron spectroscopy analysis

The line shape of Si-2p (not shown here) remains unchanged after a Fe deposition. Its intensity is rapidly attenuated and vanishes above 30 Å of Fe thickness. This is consistent with a Fe overlayer that covers uniformly the GaSe epilayer. The GaSe acts not only as a template to absorb the mismatch strain between Fe and the Si substrate through a van der Waals gap, but is also efficient to block the chemical reactivity between Si and Fe overlayers.

The Ga-3d core-level evolution is shown in Fig. 4, which displays only representative Fe coverages grown on a 20-Å-thick GaSe. The background has been subtracted for each spectra before their normalization to respect the maximum intensity corresponding to the 20-Å-thick GaSe (bottom most spectrum). In the layered compound, the Ga-3d core level is composed of one spin orbit [$3d_{3/2}-3d_{5/2}$ splitting is 0.46 eV (Ref. 27)] because Ga and Se atoms are in a single chemical environment.[28] Because of our experimental resolution, the Ga-3d line shape can be described with a single Gaussian component. No change was observed in the Ga-3d peak for the first Fe monolayer coverage, suggesting that the Fe atoms do not induce chemical disruption on the GaSe surface. The intensity decay suggests a uniform wetting of Fe over GaSe despite RHEED results, which reveals a surface roughness at an early stage of the iron coverage. Above 2 Å, the Ga-3d peak becomes clearly broadened and an extra component at 1.2 eV lower binding energy becomes visible. The relative intensity of this component increases as a function of the Fe thickness. A change in this core-level binding energy suggests that the chemical environment of some Ga atoms is modified. Thus, an extra component has been added to fit the Ga-3d core-level spectra; i.e., components represent the total emission of Ga-3d (open circles), unreacted (squares), and reacted (triangles) components. The core-level line-shape fit has been performed using a standard least-squares-fitting routine. The fitting parameters of the unreacted component were kept constant in respect to the ones from the 20-Å GaSe/Si(111); only the Gaussian width of the reacted component has been allowed to increase a little. This is justified by taking into account the interface bonding inhomogeneities.

A chemical environment modification of the Ga sites has been revealed by the Ga-3d line shape. By following the intensity attenuation, one can deduce the depth distribution of Ga atoms within the Fe overlayer. In the inset of Fig. 4, such attenuation curves have been plotted as $\ln[I_i(\theta)/I(0)]$ versus equivalent Fe coverage, where $I(0)$ is the integrated intensity taken from the 20-Å GaSe epilayer and $I_i(\theta)$ is the integrated intensity of component i. As can be seen, emission from gallium of the nondisrupted GaSe (squares) monotonously decays while the emission from the Ga-reacted com-

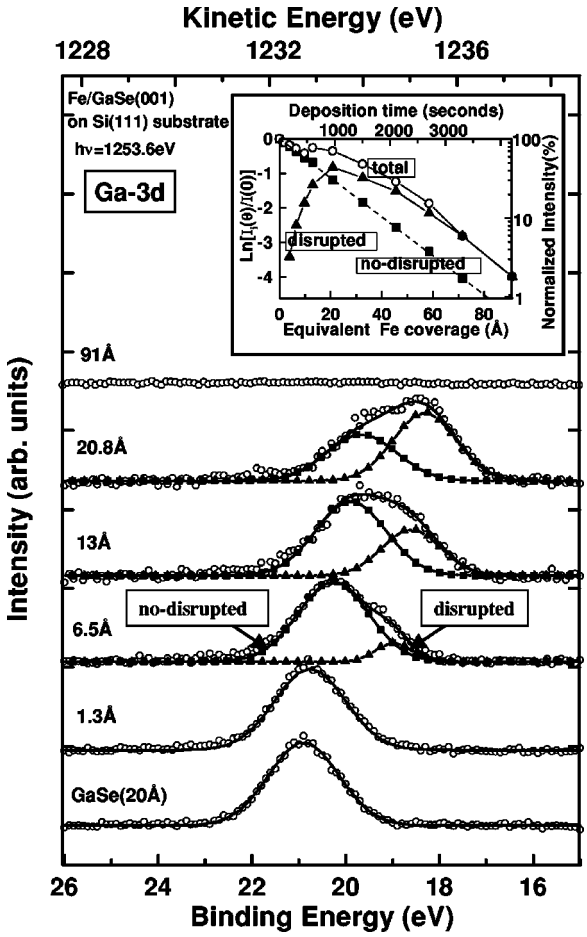

FIG. 4. Photoemission spectra of the Ga-3*d* core region recorded as a function of Fe coverage onto a 20-Å-thick GaSe epilayer on Si substrate. Only GaSe epilayer (in bottom) and representative Fe coverage are shown. For all spectra, the background was subtracted and the intensity was normalized to the maximum of the intensity corresponding to the 20-Å-thick GaSe epilayer. The collected spectra (open circles) were fitted by adjusting two Gaussian components: one associated with Ga atoms in the nondisrupted GaSe (squares) and the other with Ga-reacted atoms released from the dissociation of the topmost GaSe sheets (triangles). In the inset are shown the relative changes of the intensities of the collected Ga-3*d* signal and their two components. Our plot displays $\ln[I_i(\theta)/I(0)]$ versus equivalent Fe coverage (deposition time is given in top axis), where $I_i(\theta)$ is integrated intensity of peak *i* at coverage θ and $I(0)$ is the total Ga-3*d* integrated intensity for 20-Å-thick GaSe. The Ga photoemission associated with nondisrupted GaSe (squares) follows a layer-upon-layer growth mode (dashed line) as expected.

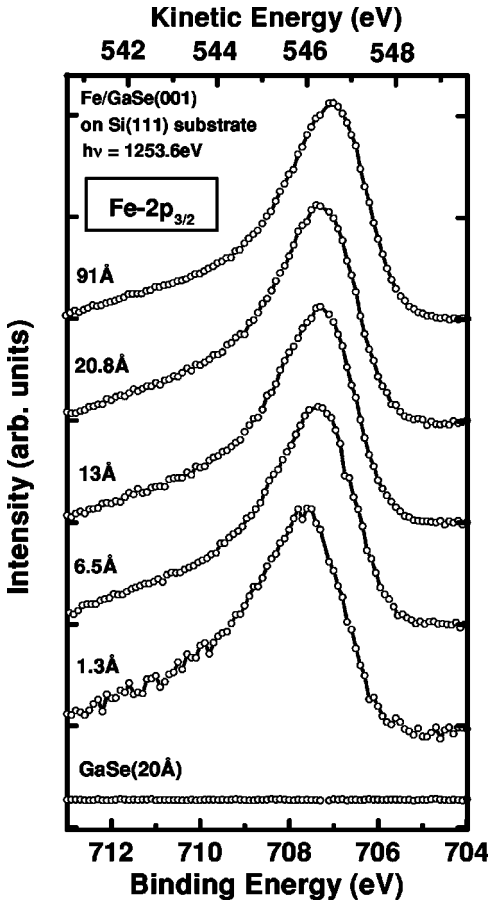

FIG. 5. Photoemission spectra of the Fe-$2p_{3/2}$ core region for Fe on 20-Å-thick GaSe(001) taken at the same Fe coverage shown in the figure of the Ga-3*d* photoemission spectra. For all spectra, the background was substracted and the intensity was normalized to the maximum of the intensity corresponding to the 91-Å-thick Fe overlayer.

ponent presents a maximum as a function of Fe coverage. By comparing the attenuation of the nondisrupted GaSe component with an exponential attenuation model (reported in the dashed lines and calculated by assuming a Ga-3*d* photoelectron mean free path of ~17.6 (Å), the Fe growth follows a layer-by-layer mechanism in spite of the dissociation of the topmost sheet of the GaSe epilayer. In the other hand, the emission from reacted Ga atoms (disrupted component) seems to support the model of self-limited GaSe disruption. For the 20.8-Å-thick Fe film, the integrated signal of the disrupted component reaches 40% of the initial Ga signal, which corresponds to two atomic planes from the five original ones. This implies that dissociation is limited to the GaSe topmost sheet from the 20-Å GaSe epilayer. Increasing the Fe film thickness, the Ga-reacted signal is attenuated faster and asymptotically superimposes the total emission decay, indicating once again, the limitation of the reacted zone.

The Se behavior shows a different feature than the Ga one. Once Se is released by the same process associated with Ga atoms, the Se-3*p* emission line shape remains unchanged as a function of the Fe coverage suggesting that within the intrinsic sensitivity of the XPS measurements, a chemical reaction between the Se and Fe epilayer is not observed. The persistence of the Se signal much beyond 91 Å of Fe clearly attests that Se segregates at the growth front, probably acting as a kind of surfactant. This has also been reported in recent work by Bourgognon *et al.* in the epitaxy of Fe or FePd on a ZnSe epilayer, where a Se floating monolayer was always observed.[29]

The Fe-$2p_{3/2}$ spectra are shown in Fig. 5 for the same Fe coverages reported in Fig. 4. It is known that in ferromagnetic iron, the Fe-2*p* core level is usually constituted by an

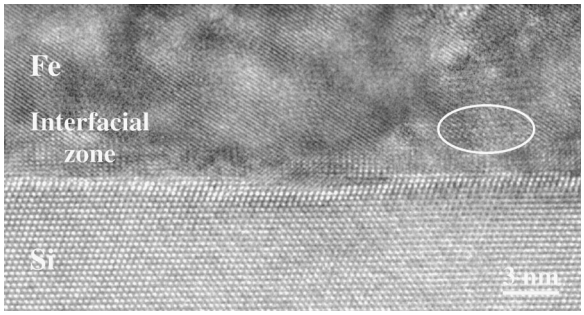

FIG. 6. HRTEM cross section of a sample ZnSe/Fe(150 Å)/GaSe(12 Å)/Si. Note the epitaxial relationship between Si, GaSe, and Fe. In the Fe layer, only one family of planes can be imaged with the 1.9-Å resolution of the equipment. Circled zone is a patterned contrast characteristic of precipitates or alloyed phases, present in high density in the vicinity of the interface.

asymmetric line shape interpreted in terms of the electron-core hole excitations across the Fermi level.[30] In fact, as shown for some Fe-$2p_{3/2}$ spectra, we find only an asymmetric line shape broadening at a higher binding energy consistent with a metallic character even at the first stage of Fe deposition. However, for sufficiently low coverage a small tail effect is observed in the line shape at higher binding energy (second spectrum from bottom to top of Fig. 5). This behavior could be correlated with island formation and the onset of the metallic character of the deposited Fe overlayer, because neither dissociation of the GaSe surface is occurring from XPS analysis nor is residual straining associated with the lattice mismatch apparent from the RHEED profile.

The overall XPS results can be understood by assuming the formation of iron gallium alloying with trapping of the released Ga atoms in a reaction region nearby the Fe/GaSe interface. Since no more than two Ga atomic planes seem to be released in the reacted zone (the XPS signal is peaked at 20.8-Å thick of Fe and smeared out up to 91-Å thick of Fe) a Fe-rich content is expected for this Fe-Ga alloying.[31] However XRD and RHEED analyses do not show evidence of a solid phase or metastable surface phase originating from nonstandard thermodynamic equilibrium in a two-dimensional structure. The formation of a solid solution with weak dilution of Ga atoms into a Fe sublayer could be invoked, but magnetic measurements discussed in the next section reveal a strong reduction of the Fe magnetic moment for very thin Fe layers. Thus, a most probable picture is that the Ga atoms incorporate into microscopic patches embedded in a Fe matrix in which the local magnetism of Fe atoms could be strongly changed. Here, it is important to emphasize that a weak selenization of the Fe film and the existence of micropatches cannot be excluded. In the next section, we investigate the interfacial zone by cross-sectional TEM.

C. Transmission electron microscopy observations

A trilayer ZnSe/Fe(150 Å)/GaSe(12 Å)/Si has been prepared by ion milling for the TEM observation in cross section along a silicon ⟨110⟩ axis. A Topcon 002B working at 200 kV has been used that gives a nominal spatial resolution of 1.9 Å. In the cross-sectional image of Fig. 6, the interfacial layer appears to be discontinuous: in some parts, the nominal thickness of the GaSe deposited is not visible, while in others, its apparent thickness is about 40 Å. The structure in these parts appears also to vary in high-resolution TEM (HRTEM) images, perhaps due to ion-beam damage during sample thinning. Above the interface layer, electron diffraction confirms that the Fe layer is indeed perfectly monocrystalline and [111] oriented, with an in-plane rotation of 180° with respect to the Si substrate (twin orientation). In the vicinity of the Si interface, the Fe layer includes nanometer-sized grains of other phases, with a density in the $10^{12}\,\mathrm{cm}^{-2}$ range. These grains have different shapes, structures, and contrasts, which indicate that the composition may also vary from one to the other. However, a majority of them just show up as a simple superstructure on the Fe lattice (Fig. 6), which shows that they are in full 3D epitaxial relationships with the Fe matrix. The Fourier transform of the circled zone in Fig. 6 gives, for example, a diagram resembling the (110) projection of Si (in a twin orientation with respect to the substrate) with a lattice parameter larger than that of Si by 2–3%. Such a pattern matches the Joint Commission for Powder-Diffraction Standard files for tetragonal $FeGa_2Se_4$. Qualitative energy dispersive x-ray spectroscopy confirms that in this interfacial zone the Fe layer contains a few percent of Ga and Se. In the next section, we address the influence of the buried-reactive zone close to the interface on the magnetic properties of the Fe films.

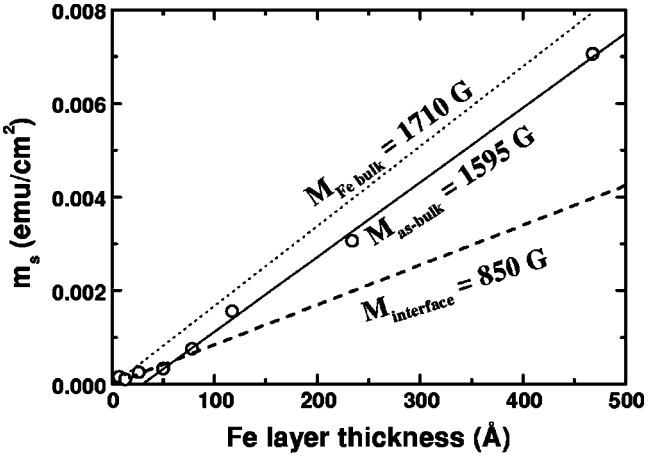

FIG. 7. Saturation magnetic moment per cm^2 versus Fe thickness. Solid line is a linear fit assuming that m_s increases linearly with the Fe thickness. Dotted and dashed lines have a slope equal to that of bulk Fe and interfacial magnetizations, respectively.

D. Magnetic properties

Magnetic measurements were performed at 30 K by using the SQUID magnetometer. The saturation magnetic moment per cm^2 (m_s) versus Fe thickness is shown in Fig. 7. In a first crude interpretation we would assume that m_s increases linearly with the thickness (solid line in Fig. 7). This leads to a solid line obtained by a linear fit whose slope (1595 G) is a magnetization value 6.7% smaller than the bulk Fe magnetization (1710 G). The extrapolation of the line intercepts the thickness axis at a value of about of 30 Å, which will lead to

the existence of an equivalent magnetically dead layer. However, it is very clear in Fig. 7 that m_s deviates from this linear behavior in the thinner thickness range. For thickness below ~60 Å, m_s is reasonably proportional to the Fe thickness but with a slope of about 850 G (see dashed line in Fig. 7). Therefore, a more advanced interpretation needs an interfacial layer, nearly half magnetized with respect to bulk Fe, covered by a bulk Fe layer with a magnetization loss of 6.7% as compared to the bulk Fe magnetization. This interfacial magnetization loss below ~60 Å clearly corroborates with the above XPS analysis, which indicates an interfacial chemical reaction between Ga and Fe in the same thickness range. Certainly, the chemical reaction started near the Fe/GaSe interface is correlated with this change of the trend magnetization at the interfacial layer. The significant reduction of the magnetic Fe moment for Fe film thicknesses below ~60 Å suggests that the buried-reactive zone with Ga atoms is strongly detrimental for the local Fe moment.

Our results also suggest an asymptotic ''as-bulk'' behavior with a magnetization of 1595 G instead of the bulk Fe magnetization (1710 G). This significant reduction of the ''as-bulk'' Fe magnetization can be attributed to either unavoidable uncertainty of the effective thickness of the Fe film or to a selenization process of the Fe films. If one assumes a slope that gives the bulk Fe magnetization (dotted line in Fig. 7), one would obtain an ideal thickness calibration. In this case, the Fe thickness would be overestimated at least by 25 Å. Such inferred error in the Fe thickness seems high in comparison to the thickness value obtained by the TEM image. On the other hand, the presence of Se atoms inside the Fe overlayer could also be related to the reduction of the observed ''as-bulk'' magnetization as compared to the bulk Fe magnetization. However, according to our XPS analysis it seems that Se is acting as a surfactant rather than promoting a selenization process of the Fe film at elevated substrate temperatures, as reported by Takahashi *et al.*[32]

Therefore, the magnetization deficiency (6.7%) observed for ''as-bulk'' Fe layers seems to be an effect of the ''weight'' of the reacted layer in the total thickness of the Fe film rather than an eventual selenization process of Fe films or thickness calibration error.

Magnetic measurements were also performed using an alternating-gradient force magnetometer operating at 300 K. In Fig. 8, the coercive field (H_c) is shown versus Fe layer thickness. Three illustrative hysteresis loops are shown in the inset of the figure. Clearly, the thickness evolution of H_c depicts a drastic change of behavior around $t_{\mathrm{Fe}}=78\,\text{Å}$. Above $t_{\mathrm{Fe}}=78\,\text{Å}$, H_c decreases almost linearly with the reciprocal Fe thickness. Since H_c reflects the volume distribution of the pinning centers for the magnetic domains in the films, such as magnetic inclusions, it is suggested that the number of pinning centers remains almost constant per unit area of the Fe films. All Fe films present ferromagnetic hysteresis loops at room temperature with remanences above 80%. The in-plane magnetic anisotropy does not differ appreciably for magnetic fields applied along the $[1\bar{1}0]$ and $[11\bar{2}]$ axes of the Si substrate, as expected for bulk α-Fe(111).

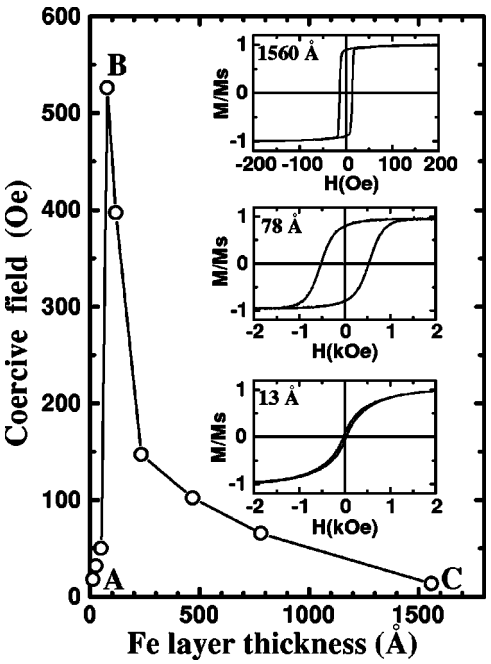

FIG. 8. Coercive field as a function of the Fe layer thickness. Magnetic measurements were performed using an alternating-gradient force magnetometer operating at 300 K with the magnetic field applied along the in-plane $[1\bar{1}0]$ direction of the Si substrate. The labels *A*, *B*, and *C* are indicating the Fe layer thicknesses (13, 78, and 1560 Å, respectively), and their hysteresis loops are shown in the inset.

Below $t_{\mathrm{Fe}}=78\,\text{Å}$, the hysteresis loops dramatically change. H_c diminishes with the decrease in the Fe thickness, whereas hysteresis loops with higher saturation fields and remanence below 10% have been observed (see bottommost hysteresis loops). In principle, deep changes could be expected in the magnetism of a Fe layer if its thickness becomes comparable to the roughness height. However, the three-dimensional diffraction reflects a small surface roughening of the Fe film, such as discussed in Sec. IIIA. Following this, roughness cannot be responsible for strong modifications in the magnetic coupling and ferromagnetism. Thus, the buried-reacted layer is more likely to be acting as a detrimental factor for the ferromagnetism than the ultimate surface morphology of the thinner Fe films. The measurements carried out with magnetic fields applied in plane and out of plane suggest that the spontaneous magnetization remains in the film plane. Additionally, for $t_{\mathrm{Fe}}<78\,\text{Å}$ a negligible in-plane magnetic anisotropy is observed, whatever in-plane direction of the applied magnetic field. Eventual antiferromagnetic behavior of the byproducts of the chemical reaction near the Fe/GaSe interface could also be hidden in this magnetic response. Such a strong modification of the local magnetism of Fe atoms corroborates with the hypothesis of microscopic patches embedded in a Fe matrix.

IV. SUMMARY AND CONCLUSIONS

We have shown that epitaxial α-Fe(111) films can be grown at 120 °C on unstrained GaSe(001) epilayers grown

themselves on surface hydrogenated (111) silicon substrate. The Fe relaxation is almost immediate and the film is fully relaxed in the monolayer regime. This demonstrates that the GaSe lamellar structure is efficient to absorb the strain between the Si substrate and the Fe overlayer, even through only a few sheets of GaSe. More interestingly, a 20-Å-thick GaSe epilayer is sufficient to block the interdiffusion between Fe and Si. However, the interaction between Fe and the topmost GaSe sheet induces a Se segregation towards the Fe growth front and a chemical Fe-Ga reaction near the interface due to the metallic Ga exposure. As a consequence, nanometer-sized grains of ordered Fe alloys are revealed in the reacted interfacial layer. This interfacial layer is nearly half magnetized as compared to the bulk α-Fe magnetization; it appears in the early stage of the Fe growth and it is gradually buried by a pure iron layer that presents a nearly ''as-bulk'' magnetization.

The use of layered materials as a buffer for ill-adapted Fe-Si epitaxial growth seems to be a promising approach to integrate magnetic properties of Fe overlayers in silicon technology, but more information on the Fe interaction with the lamellar template are still needed.

ACKNOWLEDGMENTS

One of us (D.H.M.) acknowledges the Brazilian agency CAPES for partial support. We would like to thank M. Lemal for the kind help during x-ray-diffraction measurements.

*Permanent address: Departamento de Física-UFPR, Centro Politécnico C. P. 19091, 81531-990 Curitiba PR, Brasil.

[1] See, for example, J. L. Simonds, Phys. Today **48** (4), 26 (1995).

[2] G. A. Prinz, Phys. Today **48** (4), 58 (1995).

[3] G. A. Prinz and J. J. Krebs, Appl. Phys. Lett. **39**, 397 (1981); A. Filipe, A. Schuhl, and P. Galtier, *ibid.* **70**, 129 (1997); E. M. Kneedler, B. T. Jonker, P. M. Thibado, R. J. Wagner, B. V. Shanabrook, and L. J. Whitman, Phys. Rev. B **56**, 8163 (1997); Y. B. Xu, E. T. M. Kernohan, D. J. Freeland, A. Ercole, M. Tselepi, and J. A. C. Bland, Phys. Rev. B **58**, 890 (1998).

[4] G. A. Prinz, B. T. Jonker, J. J. Krebs, J. M. Ferrari, and F. Kovanic, Appl. Phys. Lett. **48**, 1756 (1986); B. T. Jonker, J. J. Krebs, G. A. Prinz, and S. B. Qadri, J. Cryst. Growth **81**, 524 (1987); B. T. Jonker, J. J. Krebs, and G. A. Prinz, J. Appl. Phys. **69**, 2938 (1991); B. T. Jonker, G. A. Prinz, and Y. U. Idzerda, J. Vac. Sci. Technol. B **9**, 2437 (1991); H. Abad, B. T. Jonker, C. M. Cotell, and J. J. Krebs, *ibid.* **13**, 716 (1995).

[5] For MnAl: J. de Boeck, W. Van Roy, C. Bruynseraede, A. Van Esch, H. Bender, C. Van Hoof, and G. Borghs, Phys. Scr., T **66**, 183 (1996).

[6] For MnGa: M. Tanaka, J. P. Harbison, J. De Boeck, T. Sands, B. Philips, T. L. Cheeks, and V. G. Keramidas, Appl. Phys. Lett. **62**, 1565 (1993); M. Tanaka, J. P. Harbison, T. Sands, B. Philips, T. L. Cheeks, J. De Boeck, L. T. Florez, and V. G. Keramidas, *ibid.* **63**, 696 (1993).

[7] For MnSb: B. L. Low, C. K. Ong, J. Lin, A. C. H. Huan, H. Gong, and T. Y. F. Liew, J. Appl. Phys. **85**, 7340 (1999); O. Rader, A. Kimura, N. Kamakura, K-S. An, A. Kakizaki, S. Miyanishi, H. Akinaga, M. Shirai, K. Shimada, and A. Fujimori, Phys. Rev. B **57**, R689 (1998); H. Tatsuoka, K. Isaji, K. Sugiura, H. Kuwabara, P. D. Brown, Y. Xin, and C. J. Humphreys, J. Appl. Phys. **83**, 5504 (1998).

[8] For MnAs: F. Schippan, A. Trampert, L. Däweritz, K. H. Ploog, B. Dennis, K. U. Neumann, and K. R. A. Ziebeck, J. Cryst. Growth **201/202**, 674 (1999); M. Tanaka, J. P. Harbison, and G. M. Rothberg, *ibid.* **150**, 1132 (1995); K. Akeura, M. Tanaka, M. Ueki, and T. Nishinaga, Appl. Phys. Lett. **67**, 3349 (1995).

[9] Y. T. Cheng, Y. L. Chen, W. J. Meng, and Y. Li, Phys. Rev. B **48**, 14 729 (1993); F. J. A. den Broeder and J. Kohlhelpp, Phys. Rev. Lett. **75**, 3026 (1995), and references therein.

[10] See, for example, E. G. Michel, Appl. Surf. Sci. **117/118**, 294 (1997).

[11] L. J. Schowalter and R. W. Fathauer, CRC Crit. Rev. Solid State Mater. Sci. **15**, 769 (1989).

[12] K. R. Heim, G. G. Hembree, and M. R. Scheinfein, J. Appl. Phys. **76**, 8105 (1994); N. Mattoso, D. H. Mosca, W. H. Schreiner, I. Mazzaro, and S. R. Teixeira, Thin Solid Films **272**, 8386 (1996).

[13] M. R. Scheinfein, K. E. Schmidt, K. R. Heim, and G. G. Hembree, J. Appl. Phys. **79**, 5056 (1996); K. R. Heim, G. G. Hembree, and M. R. Scheinfein, *ibid.* **76**, 8105 (1994).

[14] M. Eddrief, Le Thanh Vinh, C. A. Sébenne, A. Sacuto, H. Benisty, S. Debrus, and M. Balkanski, in *Proceedings of the Fourth International Conference of the Formation of Semiconductor Interfaces*, edited by B. Lengeler, H. Lüth, W. Mönch, and J. Pollmann (World Scientific, Singapore, 1994), p. 482; Le Thanh Vinh, M. Eddrief, C. Sébenne, A. Sacuto, and M. Balkanski, J. Cryst. Growth **135**, 1 (1994).

[15] A. Koëbel, Y. Zheng, J. F. Pétroff, M. Eddrief, Le Thanh Vinh, and C. Sébenne, J. Cryst. Growth **154**, 269 (1995).

[16] A. Köebel, Y. Zheng, J. F. Pétroff, J. C. Boulliard, B. Capelle, and M. Eddrief, Phys. Rev. B **56**, 12 296 (1997); N. Jedrecy, R. Pinchaux, and M. Eddrief, *ibid.* **56**, 9583 (1997).

[17] K. Amimer, M. Eddrief, and C. A. Sébenne, J. Cryst. Growth **217**, 371 (2000); K. Amimer, University Thesis, Université Montpellier II, 1998.

[18] A. Kuhn, A. Chevy, and R. Chevalier, Phys. Status Solidi A **31**, 496 (1975).

[19] Le Thanh Vinh, M. Eddrief, C. A. Sébenne, P. Dumas, A. Taleb-Ibrahimi, R. Gunther, Y. Chabal, and J. Derrien, Appl. Phys. Lett. **64**, 3308 (1994).

[20] H. Gant and W. Mönch, Surf. Sci. **105**, 217 (1981).

[21] D. H. Mosca, J. M. George, J. L. Maurice, A. Fert, M. Eddrief, and V. H. Etgens (unpublished); See also A. Contienza, S. Massidda, and A. J. Freeman, Phys. Rev. B **42**, 2904 (1990), and references therein.

[22] Joseph A. Stroscio, D. T. Pierce, M. D. Stiles, and A. Zangwill, Phys. Rev. Lett. **75**, 4246 (1995).

[23] The surface roughness of Fe films epitaxially grown on Si(111) and Si(100) at different thicknesses was also evidenced using real-time synchrotron x-ray reflectivity measurements. See for example, H. J. Kim, D. Y. Noh, J. H. Je, and Y. Hwu, Phys. Rev. B **59**, 4650 (1999).

[24] The predominance of twinned epitaxy (*B* type) in thick α-Fe/Si(111) is evidenced by transmission electron microscopy

(TEM) and by x-ray diffraction (XRD) with ϕ scans. See for example, Yang-Tse , Yen-Lung Chen, and Wen-Ju Meng, Phys. Rev. B **48**, 14 729 (1993).

[25] For Cu epitaxy on Si(111), aligned and twinned orientations were reported to be equally probable. See for example, P. Bai, G. R. Yang, L. You, T. M. Lu, and D. B. Knorr, J. Mater. Res. **5**, 989 (1990).

[26] Swanson and Fuyat, Natl. Bur. Stand. Circ. (U.S.) **539**, 3 (1955).

[27] *Photoemission in Solids II, Topics in Applied Physics*, edited by L. Ley and M. Cardona (Springer, New York, 1979), Vol. 27, p. 377.

[28] A. Amokrane, C. A. Sébenne, A. Crienti, C. Ottaviani, F. Proix, and M. Eddrief, Appl. Surf. Sci. **123/124**, 619 (1998).

[29] C. Bourgognon, S. Tatarenko, J. Cibert, L. Carbonell, V. H. Etgens, M. Eddrief, B. Gilles, A. Marty, and Y. Samson, Appl. Phys. Lett. **76**, 1455 (2000).

[30] Detailed XPS measurements suggested that the asymmetry in the Fe-$2p$ and Fe-$3s$ core-line shapes is due to the exchange interactions between core and valence electrons (main asymmetric-line peak) and an atomic multiplet structure (small satellite peak). See for example, J. F. van Acker, Z. M. Stadnik, J. C. Fuggle, H. J. W. M. Hoekstra, K. H. J. Buschow, and G. Stroink, Phys. Rev. B **37**, 6827 (1988); S. Hong, P. Wetzel, G. Gewinner, D. Bolmont, and C. Pirri, J. Appl. Phys. **78**, 5404 (1995).

[31] Thaddeus B. Massalski, *Binary Alloy Phase Diagrams* (American Society for Metals, Metals Park, OH, 1986), p. 1063.

[32] T. Takahashi, S. Kuno, N. Honda, Y. Takemura, and K. Kakuno, J. Appl. Phys. **83**, 6533 (1998).